DOI: 10.13009/EUCASS2022-7119
9TH EUROPEAN CONFERENCE FOR AERONAUTICS AND SPACE SCIENCES (EUCASS)

A Superposition Approach to Aerodynamic Modelling of a Capturing Device used for In-Air Capturing of a Reusable Launch Vehicle

Sunayna Singh[1*], Leonid Bussler[1], Steffen Callsen[1], Sven Stappert[1],
Silvania Lopes[2], Sophia Buckingham[2]

[1]DLR Institut für Raumfahrtsysteme, Bremen, Germany
**Linzer Strasse 1, 28359, Bremen, Sunayna.Singh@dlr.de*

[2]von Karman Institute for Fluid Dynamics VKI, Belgium
72 Chaussée de Waterloo, Rhode-St-Genèse B-1640, sophia.buckingham@vki.ac.be

Abstract

This study will focus on a detailed aerodynamic analysis of the capturing device used in an innovative reusable launcher recovery concept called 'In-Air Capturing'. The idea involves capturing of a Reusable Launch Vehicle (RLV) mid-air and towing it back to launch site using an aircraft. For the capture, a device is released from the aircraft when the RLV is in vicinity. The preliminary design of this device includes a 2 m long fuselage and four large fins for agility. It is capable of pitching, yawing and rolling by symmetrically deflecting horizontal, vertical and all flaps respectively. However, for 6DOF movement, the flaps must be deflected asymmetrically in the presence of angle of attack and sideslip angle. This entails the requirement for a large dataset to effectively define the aerodynamics of the system. While a broad dataset can be generated using theoretical methods, the resulting large data tables with acceptable accuracy may not be sufficient. It is possible to achieve even better accuracy through Computational Fluid Dynamics (CFD), but the computational effort required to generate the complete aerodynamic dataset is infeasible. An alternative approach to achieve a good balance in accuracy and computation time can be used by taking advantage of the axisymmetric geometry. Thus, the paper proposes a way in which numerical CFD data for symmetric flap deflections are superimposed to achieve asymmetric flap datasets. The relative deviation of this method is compared against data generated using the semi-empirical tool Missile Datcom and validated using additional CFD calculations. Anomalies and sources of possible inaccuracies are also identified.

1. Introduction

The computation of aerodynamics is one of the most critical yet challenging aspects of defining the flight dynamics of an aerospace vehicle. A common practice is to use simpler approximate models based on empirical or semi-empirical methods that provide sufficient accuracy. However, with the computing resources becoming more accessible and affordable, numerical solutions using CFD can provide the possibility of modelling complex geometries with good accuracy. Mathematical models based on Reynolds-Averaged Navier-Stokes (RANS) equation can define both steady-state and transient flows while considering viscosity and turbulence in the flow. Nonetheless, it can still be challenging to obtain data for a wide range of operating conditions due to the overall computational effort required. Therefore, there needs to be a balance between accuracy and computational effort for effective modelling. This paper examines a method to generate extended aerodynamic dataset for an axisymmetric vehicle using a limited numerical dataset from RANS calculations.

The test vehicle for this study is a capturing device specific to the application of 'In-Air-Capturing (IAC)', which is a unique reusable launcher recovery concept proposed by DLR [1]. The complete operational cycle with IAC starts with a vertical lift-off of the launch vehicle. After Main Engine Cut-Off, the reusable winged booster re-enters the atmosphere in a ballistic trajectory and slows down to a subsonic glide through atmospheric braking. Between 8 km to 2 km altitude, the final IAC manoeuvre is performed [2]. Here, a waiting capturing aircraft approaches the RLV to achieve a parallel formation with similar velocities separated by a safe distance. Then, the RLV is actively captured by a device (attached to a rope) released from the aircraft. Finally, the aircraft tows the RLV back to the landing site where it lands horizontally on an airstrip. A basic schematic of the IAC mission cycle is shown in Figure 1.

DOI: 10.13009/EUCASS2022-7119

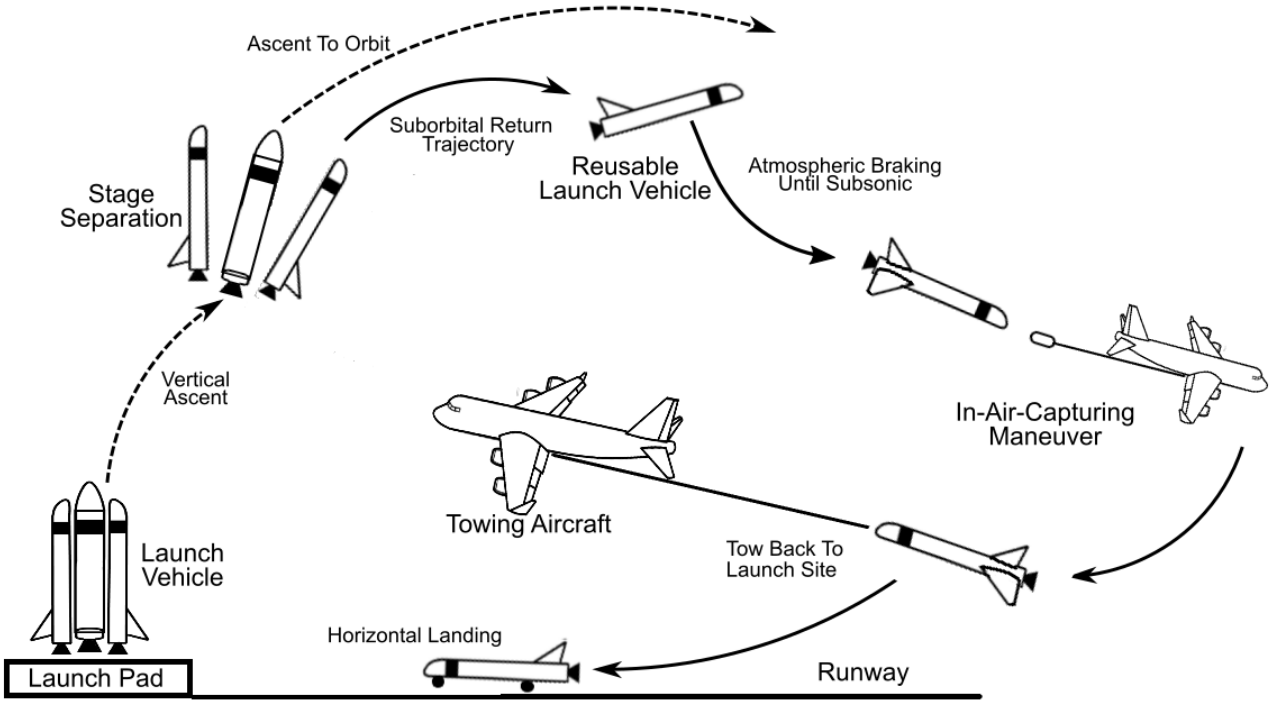

Figure 1: In-Air Capturing Mission Cycle

This study will focus on a detailed aerodynamic characterisation of the capturing device used in IAC. According to the previously studied full-scale simulations, the device should be able to manoeuvre and capture the RLV within 70 s of the formation window between the aircraft and the RLV [3]. Hence, the capturing device is required to maneouvre with agility as well as accuracy.

The most promising capturing device was found to be an Aerodynamically Controlled Capturing Device (ACCD) [4]. This device showed the best performance and agility, while posing the lowest risk. A preliminary design for ACCD is shown in Figure 2. It is a 2 m long axisymmetric body with a cross-sectional diameter of 1.5 m including the fins. The four flaps, which can deflect up to a maximum of ±15° provide 6DOF agility and control. Note that the flaps only constitute a small part of the large fins on ACCD. The nose of the ACCD is attached to the Towing Aircraft (TA) via rope and the capturing mechanism (truncated cone) at the back of the ACCD secures the connection with the RLV (using a lock-in mechanism with a boom on RLV).

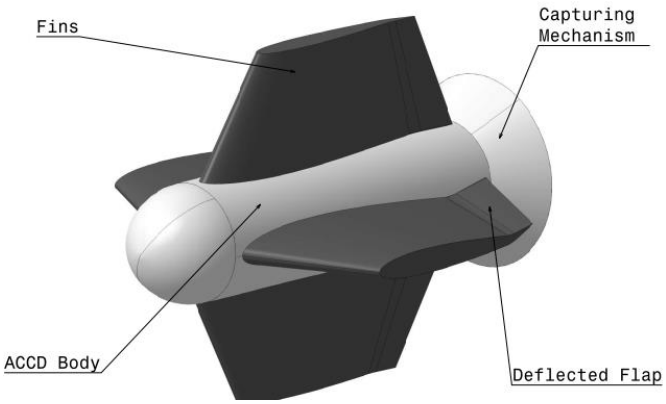

Figure 2: Aerodynamically Controlled Capturing Device

DOI: 10.13009/EUCASS2022-7119

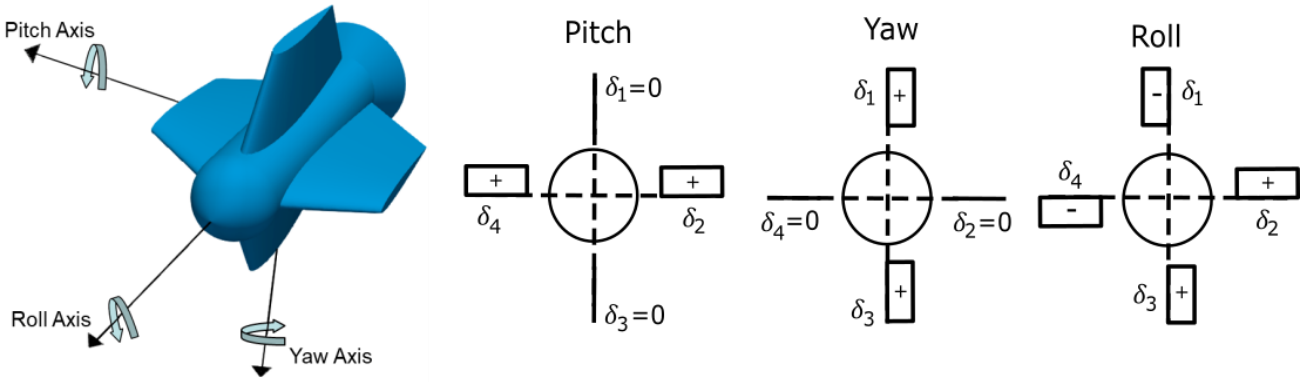

Figure 3: Conventions for ACCD Flap Deflection and the Resulting Moments

The ACCD is capable of pitching and yawing symmetrically deflecting horizontal and vertical flaps respectively [5]. Figure 3 shows a simplified representation of the sign conventions of the ACCD flaps being deflected when seen from behind. The rolling movement is achieved by deflecting all fins in either clockwise or anticlockwise direction. However, to achieve movement in more than one direction, the flaps must be deflected asymmetrically. The presence of angle of attack and sideslip angle during the flap deflection also influences the motion of the ACCD. Thus, to be able to capture 6DOF motion, the aerodynamic dataset consisting of six coefficients needs to be defined as a function of six factors:

Axial Force Coefficient:	$C_A(\alpha, \beta, \delta_1, \delta_2, \delta_3, \delta_4)$
Side Force Coefficient:	$C_Y(\alpha, \beta, \delta_1, \delta_2, \delta_3, \delta_4)$
Normal Force Coefficient:	$C_N(\alpha, \beta, \delta_1, \delta_2, \delta_3, \delta_4)$
Roll Moment Coefficient:	$C_{LL}(\alpha, \beta, \delta_1, \delta_2, \delta_3, \delta_4)$
Pitch Moment Coefficient:	$C_M(\alpha, \beta, \delta_1, \delta_2, \delta_3, \delta_4)$
Yaw Moment Coefficient:	$C_{LN}(\alpha, \beta, \delta_1, \delta_2, \delta_3, \delta_4)$

Where α is the angle of attack in degrees, β is the sideslip angle in degrees and δ is the fin deflection in degrees. The dependency on many factors leads to the requirement for a large dataset to effectively define the aerodynamics of the system. It is possible to quickly generate this broad dataset using theoretical methods, but the estimates mainly provide sufficient accuracy for preliminary simulations and need verification through numerical methods for advanced applications. Meanwhile, CFD calculations (with RANS) can provide higher accuracy but require very large computational effort to generate the complete dataset. Further, the issue of large data tables persists also with this method. An alternative approach to achieve a good balance in accuracy and computation time can be used by taking advantage of the axisymmetric geometry. The current research introduces and analyses a method based on the superposition of numerical RANS data for symmetric flap deflections (shown in Figure 3**)** to achieve asymmetric flap datasets within the dynamic model. The idea is to isolate the effect of different components like fuselage and fins from the symmetric dataset, and superpose the associated parts such that the asymmetric dataset is generated.

The methodology and numerical specifications for the RANS calculations are first introduced in Section 2. Careful consideration is put into factors like the mesh and turbulence model to achieve good accuracy. Uncertainty margins are also established based on the experimental data from a similar case study. Next, in Section 3 the control technique is introduced to get an understanding of the principle behind the proposed method. Then, the superposition approach is explained and analysed in two parts. First, as a function of angle of attack only and second, as a function of both angle of attack and sideslip angle. The relative deviation from this method is then compared against data generated using Missile Datcom and validated using additional RANS calculations. Lastly, Section 4 concludes the study.

DOI: 10.13009/EUCASS2022-7119

2. Aerodynamic Database from CFD

To take advantage of the higher accuracy of RANS calculations within the available computational limit, only symmetric configurations of the ACCD are simulated. This includes flap deflections up to ±10° in intervals of 2.5° for clean (without deflections), roll, pitch and yaw configurations as shown in Figure 3. The CFD simulations were also performed for angle of attack ranging between ±10° in intervals of 2.5°. Based on trajectory simulations from [3], the likely flight conditions for the capture of RLV were identified. Using this, a simulation flight point shown in Table 1 is established for the CFD calculations. The CFD open-source package, OpenFOAM is used to solve the compressible steady-state turbulent flow associated with this flight condition. The OpenFOAM steady state RANS compressible solver *rhoSimpleFoam* is used with second order discretization schemes to achieve higher accuracy in the results. This section briefly addresses the CFD simulation specifications and associated uncertainties for the ACCD aerodynamics.

Table 1: Simulation Flight Point for CFD

Velocity [m/s]	142.39
Mach [-]	0.45
Altitude [m]	6,000
Pressure [Pa]	47,248.92
Density [kg/m^3]	0.66065

2.1 Mesh Generation

The mesh is created with ‘snappyHexMesh’, which is a mesh generation utility of OpenFOAM, consisting of predominant hexahedral (hex) and split-hexahedral (split-hex) cells with an option of boundary layer cells insertion on the surfaces. The mesh refinement around the body can be seen in Figure 4. Three surface layers are inserted to improve the grid quality close to the body. A mesh independence analysis determined that a grid mesh size composed of 26 Million cells provided the best fit. A detailed study can be found in [6].

2.2 Turbulence Model

For the selection of an adequate turbulence model, a comparative study of three models, namely, *Spalart-Allmaras, k-epsilon* and *k-omega SST* was performed for a simple NACA0012, using the same solver [6]. For the current study, *k-omega SST* provided the best fit against the experimental data and is therefore, selected for the CFD simulations. Generally, for flight in the atmosphere the turbulent intensity is low (<1%), and only boundary layers are defined as "turbulent", having a specific effect on the flow over the object. Hence, a low turbulence intensity value of 0.5% was considered for the simulations [6].

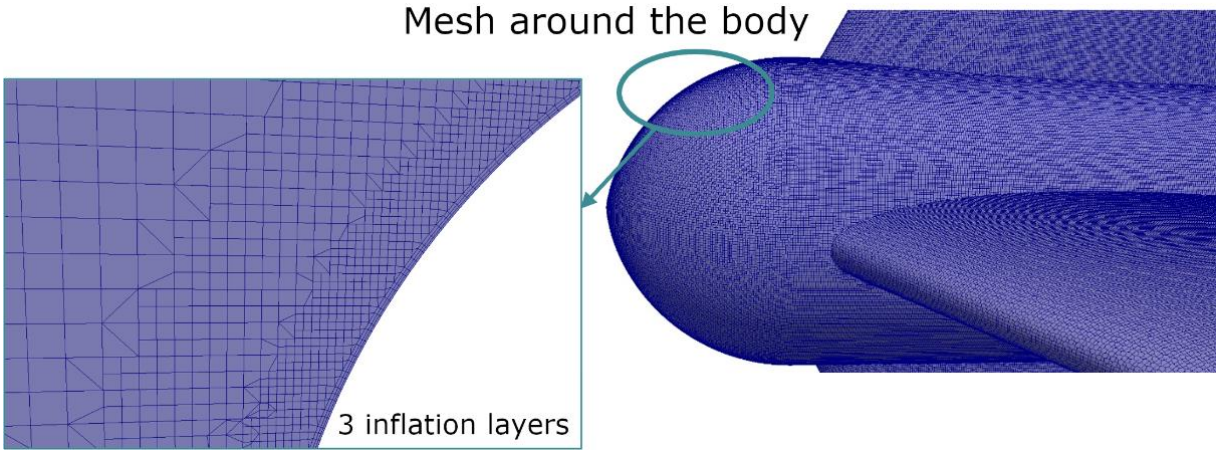

Figure 4: Mesh Refinement Around ACCD Body [6]

DOI: 10.13009/EUCASS2022-7119

In this study, the *inletOutlet* and *freeStream* boundary conditions have been used at the inlet and the outlet, respectively. The *inletOutlet* boundary condition provides a generic outflow condition, with specified inflow for the case of return flow, while the *freeStream* boundary condition provides a free-stream condition. It is a "mixed" condition derived from the *inletOutlet* condition, where the mode of operation switches between fixed (free stream) value and zero gradient based on the sign of the flux. On the interfaces between the two merged domains, a *cyclic AMI* boundary condition has been used.

2.3 Uncertainty

While generating aerodynamic datasets with CFD, many uncertainties or inaccuracies can occur. These can be linked to factors like grid independence, convergence, physical models and numerical schemes. Even though sensitivity studies are performed to achieve a high degree of accuracy, certain tolerance should be included in the computed data. To determine the uncertainty margins, the generated data needs to be compared to experimental results.

Since there were no wind tunnel experiments performed for the ACCD configuration, a comparable test case can be used as a reference. For this, the standard AGARD-B configuration (as shown in Figure 5) was chosen. This rocket like model was originally designed in 1952 by NASA and is a widely used case study for validation of subsonic, transonic and supersonic wind-tunnels around the world (Figure 6). Since the geometries are also similar, the vehicle serves as a justifiable test case. Thus, RANS simulations were performed for AGARD-B using the same specifications and the same flight point. This was then compared against the wind tunnel data for subsonic Mach numbers (0.4 to 0.6) from previous tests performed at the von Karman Institute for Fluid Dynamics (VKI) [7].

On comparing the two datasets, it was found that lift and moment coefficients were in good agreement. The drag coefficient was found to be less accurate. According to [7], the error in drag coefficient (C_D) at an angle of attack of 3° was found to be as large as 12%. The mean error in lift coefficient (C_L) at smaller angles of attack between 3° to 7° was found to be 1.8%. And the mean error in moment coefficient (C_M) for the same small angle of attack range was found to be 3.5%. On further analysis, the large discrepancies in drag coefficient was attributed to the inconsistent wall function response of the mesh. With the meshes used in AGARD-B study, the Low-Reynolds model as well as the wall functions were not well adapted for *k-omega SST*. Since the mesh is different from the ACCD mesh (due to the sharp wings and differences in geometry), the error margins obtained from this study are likely overestimated. Nonetheless, these error margins still provide a decent baseline and will be used as uncertainty margin for the CFD simulations of ACCD.

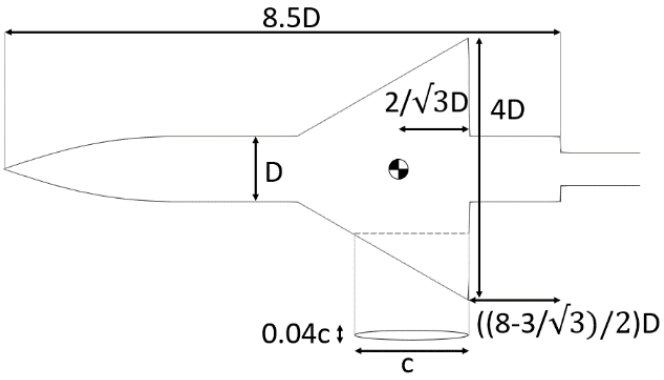

Figure 5: Section View of AGARD-B model [7]

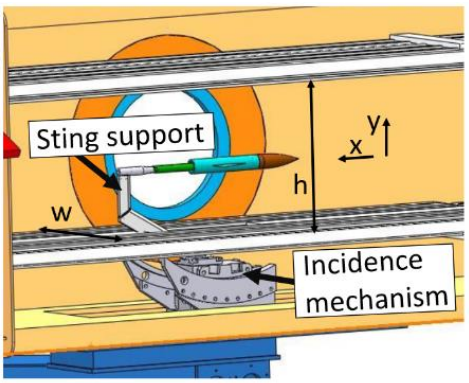

Figure 6: AGARD-B Model in Wind Tunnel [8]

DOI: 10.13009/EUCASS2022-7119

3. Superposition Approach

The superposition approach is proposed to enable the use of limited CFD dataset for quickly generating an extended aerodynamic database required for dynamic simulation. Accurate datasets can be generated for asymmetric fin deflections of ACCD by overlaying symmetric CFD data from different components. The method takes advantage of the axisymmetric geometry, providing the possibility to reduce overall computational effort. This section first introduces the principle behind the methodology, which is based on a simple control approach. Then, the approach itself is presented and evaluated for two cases. One, when only angle of attack is present and two, when both angle of attack and sideslip is present. Finally, its accuracy is examined through comparison of several asymmetric test cases generated using the proposed method with semi-empirical Missile Datcom and CFD datasets.

Missile Datcom is an aerodynamic design tool that provides the possibility to quickly generate aerodynamics for a variety of missile like configurations. It is widely used for preliminary design due to its ability to economically generate datasets with reasonable accuracy [9]. Since the ACCD geometry is an axisymmetric, elliptically shaped body with 4 fins, the tool can serve as a good standard for the superposition method. Missile Datcom also uses a similar approach like superposition, wherein the expected contributions from different components of the body like fuselage, fins and so on are combined to get the final value of the aerodynamic coefficient. The main difference between the two methods would be, that components of the coefficient are empirically estimated in Missile Datcom and superposition uses a limited CFD dataset to estimate the component contributions. Thus, Missile Datcom and CFD generated asymmetric test cases are used for the final validation of the method.

3.1 Control Approach for ACCD

The superposition approach can be directly linked to the control design of ACCD. Figure 7 shows the conventions for positive deflection of the control fins on ACCD. These four fins are deflected such that roll, pitch and yaw angles are controlled. For roll, all fins are to be deflected in the same direction (clockwise or anticlockwise). For pitch, the two horizontal fins are to be symmetrically deflected (up or down). For yaw, the two vertical fins are deflected symmetrically (left or right). Based on these conventions, the relationship can be mathematically written as:

$$\Delta p = \frac{1}{4}(\delta_1 - \delta_2 - \delta_3 + \delta_4) \tag{1}$$

$$\Delta q = \frac{1}{2}(\delta_2 + \delta_4) \tag{2}$$

$$\Delta r = \frac{1}{2}(\delta_1 + \delta_3) \tag{3}$$

A fourth combination also occurs for equation balance, but since it only generates drag and no control moments, it is not useful for control and is not mentioned here [10].

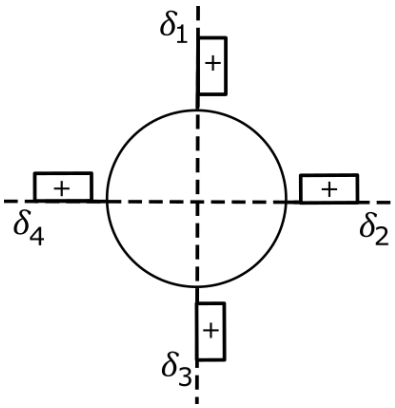

Figure 7: Positive Deflection of Control Fins on ACCD (from behind)

DOI: 10.13009/EUCASS2022-7119

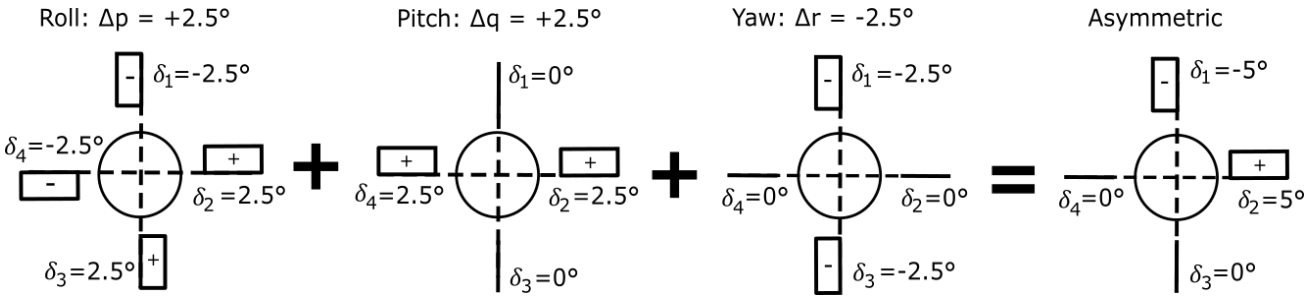

Figure 8: Simplified Representation of Asymmetric Fin Deflection of ACCD

Using the above equations, the control moments can also be directly linked to symmetric aerodynamic datasets. Thus, the aerodynamic coefficients can now be written as a function of five factors $(\alpha, \beta, \Delta p, \Delta q, \Delta r)$ instead of six factors $(\alpha, \beta, \delta_1, \delta_2, \delta_3, \delta_4)$. Since the control rates are all generated through symmetric deflections, CFD simulations are performed to create datasets for roll, pitch and yaw configurations between an angle of attack range of ±15°.

However, in reality, the ACCD is required to move in more than one direction at once. This means that the roll, pitch and yaw commands will appear at the same time. To achieve this, the fins will be required to deflect asymmetrically as shown in Figure 8. Since the symmetric deflections can be combined to get this asymmetric configuration, the aerodynamic dataset can be generated in a similar way. By separating the effect of flaps from the body (using symmetric dataset) and overlapping them according to the required configuration, the complete aerodynamic dataset can be generated within the dynamic model itself. This forms the principle of the superposition approach.

3.2 Superposition with Angle of Attack only

Similar to the control deflections, aerodynamic coefficients can also be written as a function of parameters affecting its magnitude. When only angle of attack is present (no sideslip angle), an aerodynamic coefficient can be written as a function of $\alpha, \Delta p, \Delta q, \Delta r$. This can be mathematically formulated as:

$$C_X(\alpha, \Delta p, \Delta q, \Delta r) = C_X(0) + \Delta C_X(\alpha) + \Delta C_X(\Delta p, \alpha) + \Delta C_X(\Delta q, \alpha) + \Delta C_X(\Delta r, \alpha) \quad (4)$$

Here, X is used as a generic representation since the same formula applies for all aerodynamic coefficients (C_A, $C_Y, C_N, C_{LL}, C_M, C_{LN}$). $C_X(0)$ indicates the value of coefficient when $\alpha = 0$. The symbol Δ is used to define the change in values of the coefficient. The change terms can simply be written as:

$$\Delta C_X(\alpha) = C_X(\alpha) - C_X(0) \quad (5)$$

$$\Delta C_X(\Delta p, \alpha) = C_X(\alpha) - \Delta C_X(\Delta p, \alpha) \quad (6)$$

$$\Delta C_X(\Delta q, \alpha) = C_X(\alpha) - \Delta C_X(\Delta q, \alpha) \quad (7)$$

$$\Delta C_X(\Delta r, \alpha) = C_X(\alpha) - \Delta C_X(\Delta r, \alpha) \quad (8)$$

Where $C_X(\alpha)$ indicates the value of coefficient at a given angle of attack (α), $C_X(\Delta p, \alpha)$ represents the value of coefficient at given α when roll control (Δp) is applied. Similar notations are used for pitch control (Δq) and yaw control (Δr). Thus, the aerodynamic coefficients for the asymmetric configuration shown in Figure 8, can be written using the symmetric data for $\Delta p, \Delta q, \Delta r$ at a given angle of attack. In the coming subsections, the performance of the superposition technique is compared against Missile Datcom and validated using CFD data generated for the same asymmetric configuration (-5°,5°,0°,0°).

DOI: 10.13009/EUCASS2022-7119

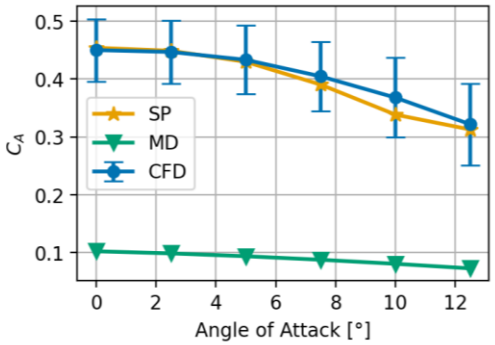

a) Axial Force Coefficient

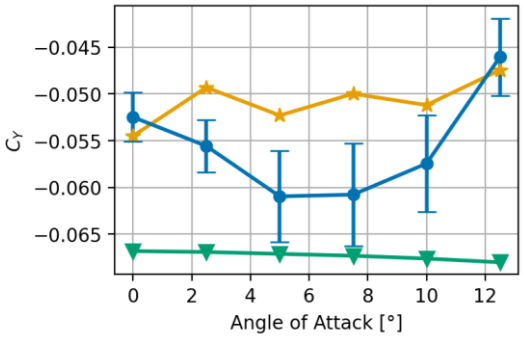

b) Side Force Coefficient

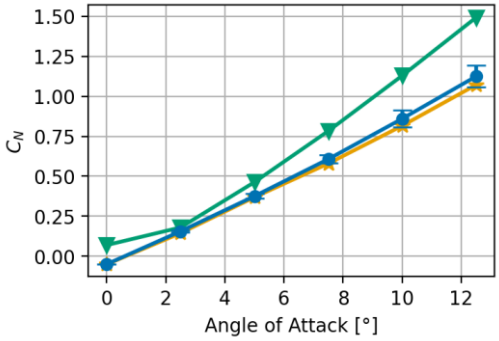

c) Normal Force Coefficient

Figure 9: Comparison of Force Coefficients for Asymmetric Fin Deflection (-5°,5°,0°,0°)

3.2.1 Force Coefficients

Figure 9 shows the comparison of the aerodynamic force coefficients for asymmetric fin deflections (-5°,5°,0°,0°) for angles of attack ranging from 0° up to 12.5°. The numerical uncertainty values of CFD as discussed in Section 2 are included as error bars in the plots. Dataset from Superposition (SP) approach generated using Equation (4) is compared against Missile Datcom (MD) and CFD data. It can be observed that SP is in very good agreement with the CFD data for the axial force coefficient as well as the normal force coefficient. In fact, for both the coefficients, SP provides a closer fit compared to MD. For side force coefficient, a maximum error of about 15% is observed at an angle of attack of 7.5°. The error can be still considered low because, the absolute difference is remains within -0.01. Therefore, for the current application, the method is still able to achieve higher accuracy than MD.

3.2.2 Moment Coefficients

Equation (4) is again used to generate the data for moment coefficients for asymmetric fin deflections (-5°,5°,0°,0°) for angles of attack ranging from 0° up to 12.5°. Figure 10 shows the comparison of the moment coefficients generated using the three methods (SP, MD, CFD). It can again be observed that SP is able to provide a good match to the reference CFD dataset for all moment coefficients (roll, pitch and yaw). The MD data when compared against the CFD appears to deviate quite a bit especially for larger angles of attack. This could be mainly attributed to the fact that Centre of Pressure (COP) moves with angle of attack and strongly depends on the flow interaction with the body. Since the SP uses data from CFD, the effect of COP movement is captured to a reasonable accuracy using SP. However, such an effect is more challenging to capture using empirical methods like MD.

DOI: 10.13009/EUCASS2022-7119

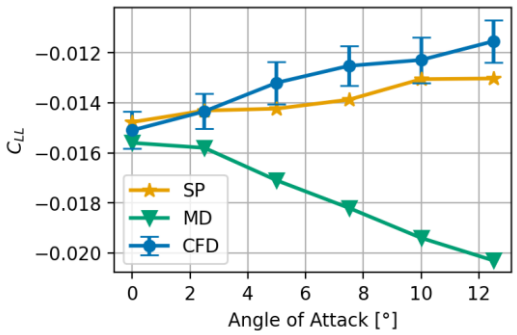

a) Roll Moment Coefficient

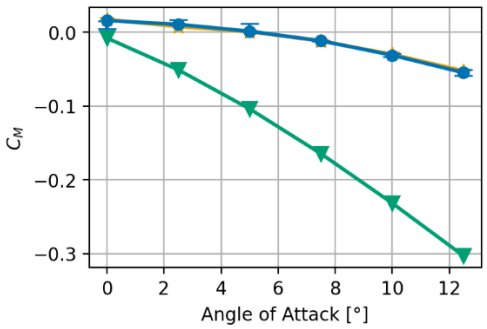

b) Pitch Moment Coefficient

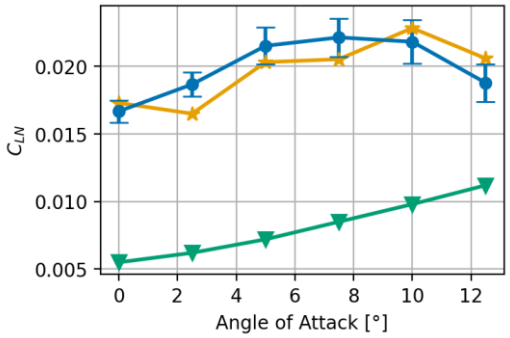

c) Yaw Moment Coefficient

Figure 10: Comparison of Moment Coefficients for Asymmetric Fin Deflection (-5°,5°,0°,0°)

3.3 Superposition with Angle of Attack and Sideslip Angle

As stated earlier, CFD simulations are performed to create datasets for roll, pitch and yaw configurations between an angle of attack range of ±15°. Taking advantage of the axisymmetric geometry of the ACCD, the dataset could then be extended to roll, pitch and yaw datasets for sideslip angles of up to ±15°. Here, the axial force coefficients and roll moment coefficients are assumed to be the same as that for angle of attack data. The force and moment coefficients along the YZ-directions, are swapped based on the symmetry. This can be simply visualized as the geometry rotated by 90°. The transition from angle of attack dataset to sideslip angle dataset can be summarised as follows:

Force Coefficients	Moment Coefficients
$C_A(\alpha) = C_A(\beta)$	$C_{LL}(\alpha) = C_{LL}(\beta)$
$C_Y(\alpha) = C_N(\beta)$	$C_M(\alpha) = C_{LN}(\beta)$
$C_N(\alpha) = C_Y(\beta)$	$C_{LN}(\alpha) = C_M(\beta)$

The two aerodynamic datasets as a function of $\alpha, \Delta p, \Delta q, \Delta r$ and $\beta, \Delta p, \Delta q, \Delta r$, can now be superposed to obtain an aerodynamic dataset as a function of $\alpha, \beta, \Delta p, \Delta q, \Delta r$. Equation (4) can thus be extended to:

$$C_X(\alpha,\beta,\Delta p,\Delta q,\Delta r) = C_X(0) + (\Delta C_X(\alpha) + \Delta C_X(\Delta p,\alpha) + \Delta C_X(\Delta q,\alpha) + \Delta C_X(\Delta r,\alpha)) * \epsilon + (\Delta C_X(\beta) + \Delta C_X(\Delta p,\beta) + \Delta C_X(\Delta q,\beta) + \Delta C_X(\Delta r,\beta)) * (1-\epsilon) \quad (9)$$

Where the notations used are similar to the one used in Equation (4). The term ϵ is a linear scaling factor given by:

DOI: 10.13009/EUCASS2022-7119

$$\epsilon = \frac{|\alpha|}{|\alpha| + |\beta|} \tag{10}$$

The change (Δ) terms for sideslip can then be defined as,

$$\Delta C_X(\beta) = C_X(\beta) - C_X(0) \tag{11}$$

$$\Delta C_X(\Delta p, \beta) = C_X(\beta) - C_X(\Delta p, \beta) \tag{12}$$

$$\Delta C_X(\Delta q, \beta) = C_X(\beta) - C_X(\Delta q, \beta) \tag{13}$$

$$\Delta C_X(\Delta r, \beta) = C_X(\beta) - C_X(\Delta r, \beta) \tag{14}$$

Where $C_X(\beta)$ indicates the value of coefficient at a given sideslip angle (β), $C_X(\Delta p, \beta)$ represents the value of coefficient at given β when roll control (Δp) is applied. Similar notations are used for pitch control (Δq) and yaw control (Δr). The aerodynamic coefficients for the asymmetric configuration shown in Figure 8, are again recalculated with Equation (9). Reference data is generated using CFD for different combinations of α and β as shown in Table 2.

Table 2: CFD Reference Datapoints for Validation of Superposition Method

α [°]	β [°]	δ_1 [°]	δ_2 [°]	δ_3 [°]	δ_4 [°]
2.5	5	-5	5	0	0
2.5	15	-5	5	0	0
5	5	-5	5	0	0
5	-5	-5	5	0	0
-5	2.5	-5	5	0	0
-15	2.5	-5	5	0	0

The datapoints stated in Table 2 will be compared using the three methods, MD, SP and CFD for validation.

3.3.1 Force Coefficients

Figure 11, Figure 12 and Figure 13 show the force coefficients calculated using SP, MD and CFD for the datapoints presented in Table 2. It can be observed that the axial force coefficient (C_A) using SP shows good agreement with the reference CFD dataset. The estimated values from SP also provide a closer match than the MD data. However, when compared against the case with α only (Figure 9), it can be observed that SP method sees larger relative errors when both α and β are present. This is expected since a linear scaling factor (ϵ) is used to determine the contributions from α and β. Additionally, uncertainties are introduced due to the assumption that aerodynamic coefficients with β can be entirely derived using symmetry and CFD dataset with α.

In Figure 12, the values of side force coefficient (C_Y) derived from SP also remain in good agreement with CFD data. A large error of about 16.5% is seen SP dataset, when $\alpha = -15°$ and $\beta = 2.5°$. This can be attributed to the fact that at larger values of α and β complex interactions may happen, which cannot be captured by the simplified superposition approach. For instance, a part of the flap may be blocked by the body, which could lead to uneven pressure distribution. Turbulent flow and flow separation at high α and β may also explain the discrepancies. Nonetheless, SP still provides a much closer fit to the reference CFD values than MD.

In Figure 13, normal force coefficient (C_N) calculated using SP provides good estimates with relative errors less than 10%. Again, values from SP provide a closer fit to reference CFD data than MD.

DOI: 10.13009/EUCASS2022-7119

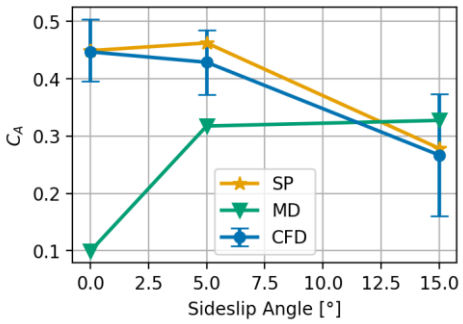

a) Axial Force Coefficient with α = 2.5°

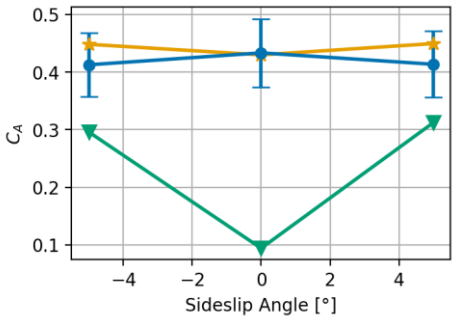

b) Axial Force Coefficient with α = 5°

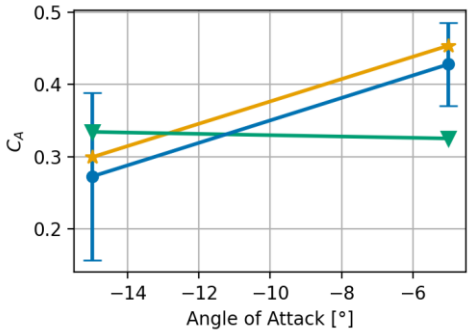

c) Axial Force Coefficient with β = 2.5°

Figure 11: Comparison of Axial Force Coefficients for Asymmetric Fin Deflection (-5°,5°,0°,0°) for both Angle of Attack and Sideslip Angle

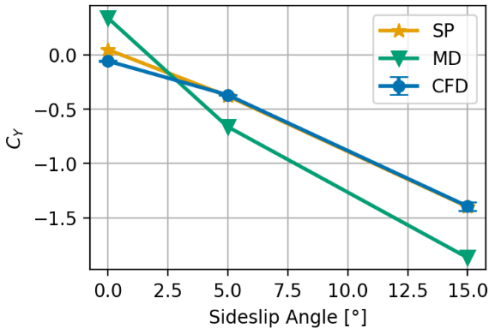

a) Side Force Coefficient with α = 2.5°

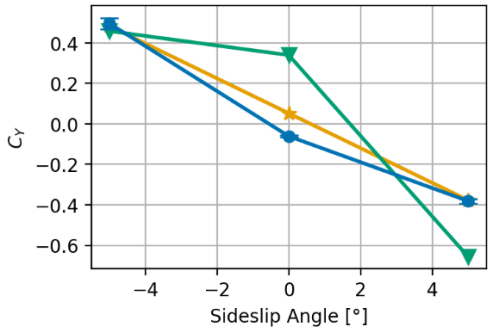

b) Side Force Coefficient with α = 5°

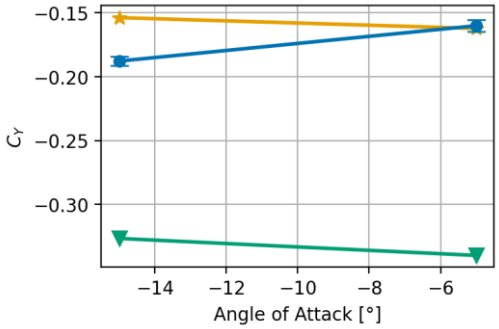

c) Side Force Coefficient with β = 2.5°

Figure 12: Comparison of Side Force Coefficients for Asymmetric Fin Deflection (-5°,5°,0°,0°) for both Angle of Attack and Sideslip Angle

DOI: 10.13009/EUCASS2022-7119

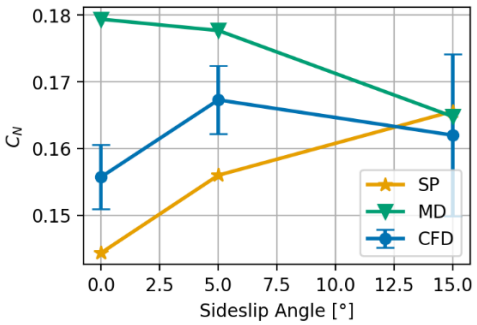

a) Normal Force Coefficient with α = 2.5°

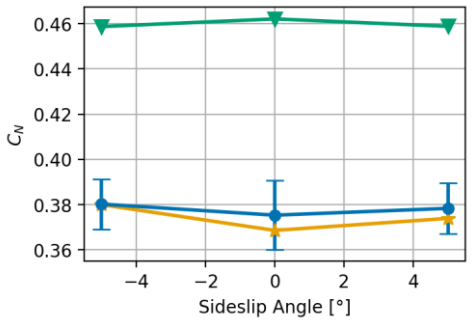

b) Normal Force Coefficient with α = 5°

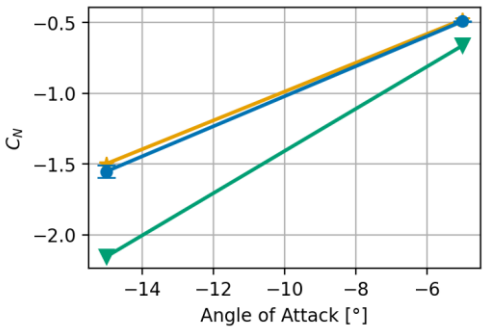

c) Normal Force Coefficient with β = 2.5°

Figure 13: Comparison of Normal Force Coefficients for Asymmetric Fin Deflection (-5°,5°,0°,0°) for both Angle of Attack and Sideslip Angle

3.3.2 Moment Coefficients

Figure 14, Figure 15 and Figure 16 show the moment coefficients calculated using SP, MD and CFD for the datapoints presented in Table 2 and the asymmetric configuration in Figure 8. It can be observed from Figure 14 that the roll moment coefficient (C_{LL}) generated using SP provide a decent estimate when β is small. As the value of β increases, the relative error against CFD also increases. The slope of the curve achieved using SP is quite comparable to MD, indicating the similarities in the approximation methods. The large errors seen in C_{LL} could be again attributed to the part that the COP position. When both α and β are present, the estimated COP from SP see larger errors than the case with α only. It could be that presence of β has a larger impact on roll moment than what is predicted using linear scaling. The assumption that $C_{LL}(\alpha) = C_{LL}(\beta)$ could also be adding to the inaccuracy. For the current application, the ACCD is required to move in the YZ-plane and the roll orientation is mainly used to determine the orientation of the fins (see [9]). Therefore, the present errors in roll moment are not as critical for the full-scale simulation of the ACCD dynamics and the SP approach remains valid for the study.

In Figure 15, the values of pitch moment coefficient (C_M) are compared. The data generated using Equation (9) is represented by SP1. Since the effect of β is likely not to have a strong impact on C_M, a SP dataset is also generated using Equation (4), ignoring the effect of β. This is marked with SP2. It can be observed that SP2 provides the closest match to the reference data. The relative errors in C_M remain on the lower side, likely because the COP along pitch is predominantly influenced by α, unlike C_{LL} which was likely influenced by both α and β. This reduces the uncertainty in prediction of moments, Moreover, a closer fit was again achieved using SP2 than using MD. Therefore, Equation (4) is used for the estimation of C_M even when both α and β are present.

Lastly, Figure 16 shows comparison of the yaw moment coefficient (C_{LN}). It can be observed that SP is able to predict most values with reasonable accuracy apart from datapoints with very high angles ($\alpha = 2.5°$ and $\beta = 15°$; $\alpha = -15°$ and $\beta = 2.5°$). This can be again attributed to the complex effects at high aerodynamic angles. Uneven pressure distribution also causes the COP to move in a non-linear way, which cannot be predicted by the simplified SP method. Preliminary simulations of ACCD performing maneouvres for capture phase shown in [11], indicates that ACCD is able to achieve the required manoeuvrability margin within an α and β range of ±5°. Since the SP method has proven to be really effective for smaller values of α and β, it can be considered relevant for the current application.

DOI: 10.13009/EUCASS2022-7119

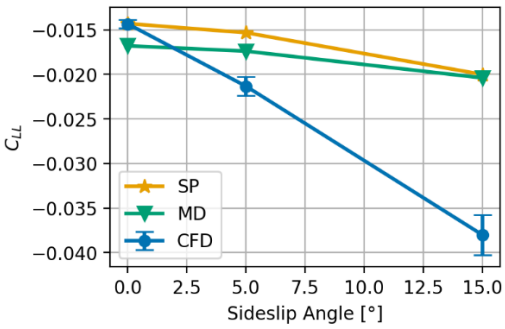

a) Roll Moment Coefficient with α = 2.5°

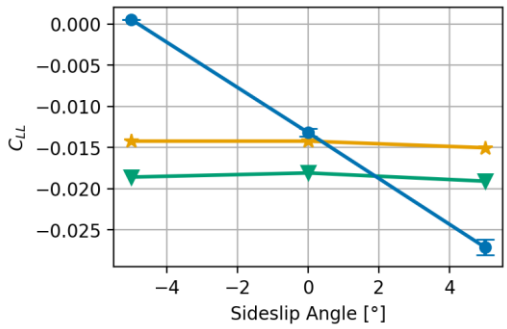

b) Roll Moment Coefficient with α = 5°

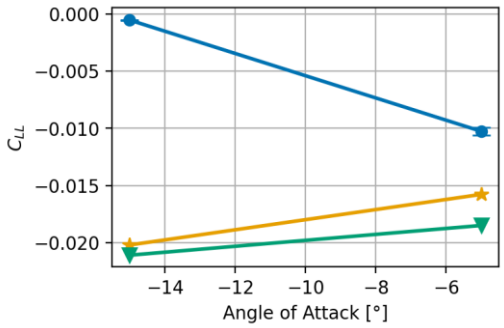

c) Roll Moment Coefficient with β = 2.5°

Figure 14: Comparison of Roll Moment Coefficients for Asymmetric Fin Deflection (-5°,5°,0°,0°) for both Angle of Attack and Sideslip Angle

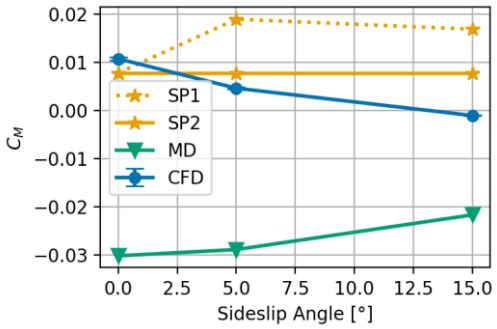

a) Pitch Moment Coefficient with α = 2.5°

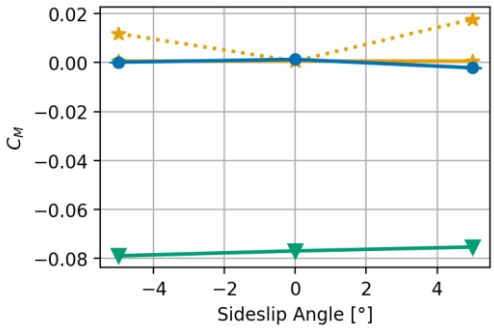

b) Pitch Moment Coefficient with α = 5°

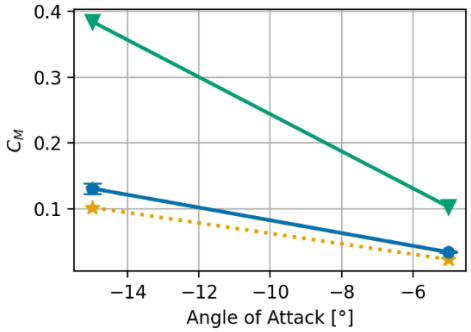

c) Pitch Moment Coefficient with β = 2.5°

Figure 15: Comparison of Pitch Moment Coefficients for Asymmetric Fin Deflection (-5°,5°,0°,0°) for both Angle of Attack and Sideslip Angle

DOI: 10.13009/EUCASS2022-7119

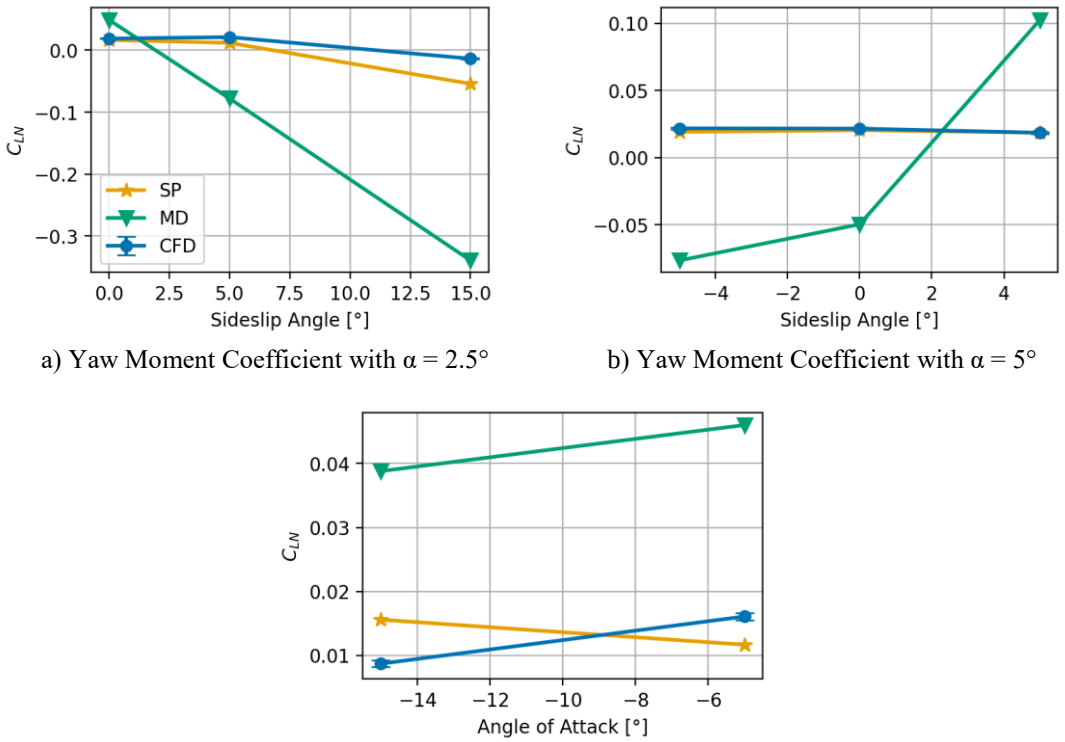

a) Yaw Moment Coefficient with α = 2.5°

b) Yaw Moment Coefficient with α = 5°

c) Yaw Moment Coefficient with α = 5°

Figure 16: Comparison of Yaw Moment Coefficients for Asymmetric Fin Deflection (-5°,5°,0°,0°) for both Angle of Attack and Sideslip Angle

4. Conclusion

This paper proposes a method for estimation of 6DOF aerodynamics of axisymmetric bodies. It relies on superposition of limited CFD datasets to generate an extended database. This enables a good balance between accuracy and computation time. The test vehicle used for evaluation of the method is a capturing device used in an innovative launcher recovery concept called 'In-Air Capturing'. The preliminary design of this device includes a 2 m long fuselage with a spherical head and four large fins for agility. It is capable of pitching, yawing and rolling by symmetrically deflecting horizontal, vertical and all flaps respectively. However, to achieve 6DOF movement, the flaps must be deflected asymmetrically in the presence of angle of attack and sideslip angles. The aerodynamic dataset for symmetric flap deflections is first generated numerically using RANS for a range of angles of attack. Then, expected contributions from different components of the body like fuselage and fins are derived from this CFD data. The aerodynamics for asymmetric flap deflections are then generated through superposition of these individual contributions. By establishing this approach within the dynamic model through simple mathematical expressions, the need for large aerodynamic tables can be eliminated.

A number of asymmetric datapoints generated using this method are compared against data from a semi-empirical tool for aerodynamics called Missile Datcom. Additional, CFD computations are also performed to validate the superposition method at these datapoints. On comparison of the three sources, it was found that the superposition approach is able to provide accurate estimates of the aerodynamic coefficients when an angle of attack range of ±15° is considered. However, when both angle of attack and sideslip angle are present, the accuracy of the approach reduces for higher aerodynamic angles. Since ACCD is able to achieve the required manoeuvrability margin using small angles of attack and sideslip angles (up to 5°), the dataset generated using this approach proves to be credible. Overall, the method is found also to be more accurate than Missile Datcom for the current application.

DOI: 10.13009/EUCASS2022-7119

Acknowledgements

This work was performed under the Horizon 2020 project '**F**ormation flight for in-**A**ir **L**auncher 1st stage **C**apturing demonstrati**on**' (**FALCon**) for development and testing of the "In-Air Capturing" technology. FALCon, coordinated by DLR-SART, is supported by the EU in the Programme 5.iii. Leadership in Enabling and Industrial Technologies – Space with EC grant 821953. Further information on FALCon can be found at http://www.FALCon-iac.eu

List of Abbreviations

Abbreviation	Definition
ACCD	Aerodynamically Controlled Capturing Device
CFD	Computational Fluid Dynamics
DLR	German Aerospace Center
6DOF	Six Degree of Freedom
IAC	In-Air Capturing
MD	Missile Datcom
RANS	Reynolds-Averaged Naviers Stokes
RLV	Reusable Launch Vehicle
SP	Superposition
TA	Towing Aircraft
VKI	Von Karman Institute for Fluid Dynamics

Nomenclature

Symbol	Description
C_L	Lift coefficient
C_D	Drag coefficient
C_A	Axial force coefficient
C_Y	Side force coefficient
C_N	Normal force coefficient
C_{LL}	Roll moment coefficient
C_M	Pitch moment coefficient
C_N	Yaw moment coefficient
Δp	Roll control rate
Δq	Pitch control rate
Δr	Yaw control rate
$C_X(Y)$	Aerodynamic coefficient specified by subscript X as a function of Y
$\Delta C_X(Y)$	Change in aerodynamic coefficient specified by subscript X as a function of Y
α	Angle of attack in [°]
β	Sideslip angle in [°]
ϵ	Scaling factor based on angle of attack and side slip angle
δa	Deflection of fin number a in [°]

References

[1] Patentschrift (patent specification) DE 101 47 144 C1, Verfahren zum Bergen einer Stufe eines mehr-stufigen Raumtransportsystems, released 2003.

[2] M. Sippel, S. Stappert, S. Singh, "RLV-Return Mode "In-Air-Capturing" and Definition of its Development Roadmap", *9th European Conference for Aeronautics and Space Sciences (EUCASS)*, 2022.

[3] S. Singh, S. Stappert, L. Bussler, M. Sippel, Y. C. Kucukosman, S. Buckingham, "A Full-Scale Simulation and Analysis of Formation Flight during In-Air Capturing", IAC-21-D2.5.2, *72nd International Astronautical Congress (IAC)*, 2021.

DOI: 10.13009/EUCASS2022-7119

[4] M. Sippel, J. Klevanski: "Progresses in Simulating the Advanced In-Air-Capturing Method", *5th International Conference on Launcher Technology, Missions, Control and Avionics*, 2003

[5] S. Singh., S. Stappert, S. Buckingham, S. Lopes, Y.C. Kucukosman, M. Simioana, M. Pripasu, A. Wiegand, M. Sippel, P. Planquart, "Dynamic Modelling and Control of an Aerodynamically Controlled Capturing Device for 'In-Air-Capturing' of a Reusable Launch Vehicle", *11th International ESA Conference on Guidance, Navigation & Control Systems*, 2021.

[6] S. Lopes, Y. C. Kucukosman, S. Buckingham, "FALCon Deliverable D7.1 Part 1: CFD Study of Full-Scale Vehicles", EC project number 821953, 2022.

[7] R. Poletti, "Proof of Concept by CFD for an Aerodynamically Controlled Capturing Device", von Karman Institute for Fluid Dynamics, 2019.

[8] S. Paris, J. van Beeck, J. Ramos, T. Regert. "First Characterization of the VKI S1 Wind Tunnel by Means of the AGARD-B Model", von Karman Institute for Fluid Dynamics, 2015.

[9] C. Rosema, J. Doyle, L. Auman, M. Underwood, "Missile Datcom User Manual", 2011.

[10] P. H. Zipfel, "Modelling and Simulation of Aerospace Vehicle Dynamics", Second Edition, 2007.

[11] S. Singh, L. Bussler, S. Stappert, M. Sippel, S. Buckingham, S. Lopes, C. Y. Kucukosman, "Control Design and Analysis of a Capturing Device Performing In-Air Capturing of a Reusable Launch Vehicle", *9th European Conference for Aeronautics and Space Sciences (EUCASS)*, 2022.